Master's Thesis

A Numerical Study of the Characteristics of Autoignited Laminar Lifted Methane/Hydrogen Jet Flames in Heated Coflow air

Ki Sung Jung

Department of Mechanical Engineering

Graduate School of UNIST

2018

A Numerical Study of the Characteristics of Autoignited Laminar Lifted Methane/Hydrogen Jet Flames in Heated Coflow air

Ki Sung Jung

Department of Mechanical Engineering

Graduate School of UNIST

A Numerical Study of the Characteristics of Autoignited Laminar Lifted Methane/Hydrogen Jet Flames in Heated Coflow air

A thesis/dissertation

submitted to the Graduate School of UNIST

in partial fulfillment of the

requirements for the degree of

Master of Science

Ki Sung Jung

December. 06. 2017

Approved by

Advisor

Chun Sang Yoo

A Numerical Study of the Characteristics of Autoignited Laminar Lifted Methane/Hydrogen Jet Flames in Heated Coflow air

Ki sung Jung

This certifies that the thesis/dissertation of Ki Sung Jung is approved

06/Dec/2017

Signature

Advisor: Chun Sang Yoo

Signature

Hyungson Ki

Signature

Taesung Kim

Abstract

In this thesis, the characteristics of autoignited laminar lifted jet flames of methane/hydrogen binary mixture fuels in heated coflow air are numerically investigated using laminarSMOKE with a 30-species skeletal methane/air kinetic mechanism. Detailed numerical simulations are performed for various fuel jet velocities with different hydrogen ratio of the fuel jet and the inlet temperature. Based on the flame structure and ignition temperature, the autoignited laminar lifted jet flames can be categorized into three different regimes of combustion mode: the tribrachial edge flame regime, the Moderate or Intense Low-oxygen Dilution (MILD) combustion regime, and the transition regime in between. Under relatively low temperature and high hydrogen ratio (LTHH) conditions, the simulations can capture an unusual decreasing liftoff height behavior with increasing jet velocity, qualitatively similar to those of previous experimental observations. From additional simulations with modified hydrogen mass diffusivity, it is verified that the high diffusive nature of hydrogen molecules is primarily attributed to the unusual liftoff height behavior under the LTHH condition. The Damköhler number analysis, transport budget analysis and chemical explosive mode analysis (CEMA) verify that autoignition in the region upstream of the flamebase plays a critical role in stabilizing the lifted jet flames. In addition, the CEMA also identifies important species and reaction steps for the autoignition in the MILD combustion and tribrachial edge flame regimes. Finally, a novel correlation for the prediction of liftoff height is proposed for the autoignited laminar lifted methane/hydrogen jet flames under the LTHH conditions by noting that the ignition delay determined based on the species components at the flamebase can represent the autoignition of the binary mixture fuel jet reasonably well. The new correlation shows good agreement with the simulation results.

Contents

List of Figures

List of Tables

1. Introduction

Reducing pollutant emission is one of the most important issues to be solved in combustion society, and compressed natural gas (CNG) is therefore highlighted as a suitable alternative fuel because natural gas is plentiful in the world, and it emits less pollutants as compared to the other fossil fuels [1]. Regardless of the advantage of natural gas, however, natural gas itself is not commonly used in the practical combustion applications because of its low ignitability, and high autoignition temperature. Natural gas consists primarily of methane (CH_4) and small amounts of other alkanes, and breaking the molecular bonds of CH_4 requires much energy because of the stable molecular structure of CH_4.

In this regard, various types of species are blended with the natural gas to cope with the limitation of methane combustion on the real appliances, and hydrogen has been a recent research interest as an additive on the methane combustion because of the hydrogen's special characteristics as shown in Table 1 [2, 3]. For example, the laminar flame speed of hydrogen is approximately 7 times faster than that of methane, which leads the increase of the burning velocity of the mixture [4]. Additionally, due to the hydrogen's low lean-flammability limit, the methane/hydrogen mixtures can be operated under the highly diluted condition which in turn improving engine emissions [5].

Table 1. Fuel properties of methane and hydrogen

Properties	Methane (CH_4)	Hydrogen (H_2)
Quenching distance (mm)	1.9	0.6
Density at NTP (kg/m^3)	0.754	0.082
Stoichiometric air-fuel ratio (% by volume)	9.396	2.387
Laminar burning velocity (m/s)	0.38	2.9
Volumetric lower heating value (MJ/ m^3)	32.97	10.22
C/H ratio	0.2514	0

With the increasing demand on the hydrogen enriched natural gas combustion (HCNG or H_2CNG) in many practical combustion appliances such as diesel engines and homogenous charge compression ignition (HCCI) engine, we focus on the detailed autoignition characteristics of the laminar lifted methane/hydrogen jet flames in heated coflow air.

In general, autoignition in an ideal HCCI engine occurs under adiabatic condition due to its homogeneities in both temperature and composition. However, autoignition in variants of HCCI combustion including stratified charge compression ignition (SCCI) and reactivity controlled compression ignition (RCCI) combustion occurs non-adiabatically due to their mixture stratification

and/or direct-fuel injection to control overall ignition timing and mitigate excessive pressure rise rate (PRR) in an engine cylinder [7-16]. Similarly, autoignition in the diesel combustion occurs non-adiabatically due to its inherent mixture stratification. Therefore, the liftoff characteristics and stabilization mechanisms of turbulent lifted jet flames at high pressures and high temperatures have been a long-time research topic to understand the fundamentals of the diesel combustion [17-21].

The characteristics of autoignited laminar lifted jet flames in heated coflow air have also been widely investigated due to their distinct features from those of non-autoignited lifted jet flames and their potential as a building-block configuration for understanding the stabilization of turbulent lifted jet flames at high pressures and temperatures as in the diesel combustion [22-30]. Chung and co-workers [22-24] found that an autoignition kernel in laminar non-premixed fuel jet in heated coflow air can develop into a stationary lifted flame or a nozzle-attached flame depending on the inlet conditions of the fuel jet and coflow air. They also elucidated that a stable autoignited laminar lifted flame can exist regardless of the Schmidt number of the fuel jet, *Sc*, whereas a stationary non-autoignited lifted flame exists only for the fuels which *Sc* is greater than unity in a free jet [31,32].

The autoignited laminar lifted flame can be subcategorized into the lifted flame with tribrachial edge or Moderate of Intense Low-oxygen Dilution (MILD) combustion depending on the initial fuel mole fraction $X_{F,0}$. The lifted flame with tribrachial edge exists when the fuel ratio in fuel jet, $X_{F,0,}$ is relatively high, and its leading edge consists of rich/lean premixed flame wings and a trailing non-premixed flame [28] as shown in figure 1. Lifted flame with MILD combustion, on the other hand, it exists when the fuel jet is highly diluted with an inert gas such as nitrogen (relatively low $X_{F,0}$). Overall flame structure of MILD combustion does not exhibit the conventional tribrachial edge flame and its features the faint blue color without exhibiting a clear tribrachial structure [22-24, 28]. Recently, Deng et al. [29, 30] researched the liftoff and flame structure characteristics of laminar lifted DME jet flames and suggested a regime diagram for classifying the stabilization mechanism of lifted flame depending on the inlet temperature and jet velocity.

From the previous experimental researches on the autoignited laminar lifted flames [22, 23], liftoff height H_L variation of the various kinds of single fuel (e.g., methane, propane) was intensively studied. Under the autoignition of lifted flame with tribrachial edge, H_L of laminar lifted flames was successfully correlated as functions of fuel jet velocity, U_0, and the 0-D adiabatic ignition delay time of the stoichiometric fuel/air mixture at the fuel/coflow jets, $\tau_{ig,st}$: $H_L \sim U_0 \tau_{ig,st}^2$. This correlation was originally devised by Choi et al. [22] considering the thermal balance between heat release from autoignition and heat loss by diffusion at the jet mixing layer. Therefore, it is noted that H_L generally increases with the increase of U_0 under the same inlet condition because $\tau_{ig,st}$ remains constant with the U_0 change. This correlation shows good agreement with experiments for autoignited lifted flames

with tribrachial edge structure of various single component fuel jets [23]. For the lifted flame with MILD combustion, a revised correlation was derived by multiplying the mass fraction of fuel in the fuel jet, $Y_{F,0}$: $H_L \sim Y_{F,0} U_0 \tau_{ig,st}^2$, [23] which is incorporating the ignition strength of the fuel jet. For both H_L correlations of tribrachial edge flame and MILD combustion, we can readily observe a quadratic dependence of H_L on $\tau_{ig,st}$, which implies that the adiabatic 0-D ignition delay can play a critical role in stabilizing autoignited laminar lifted jet flames.

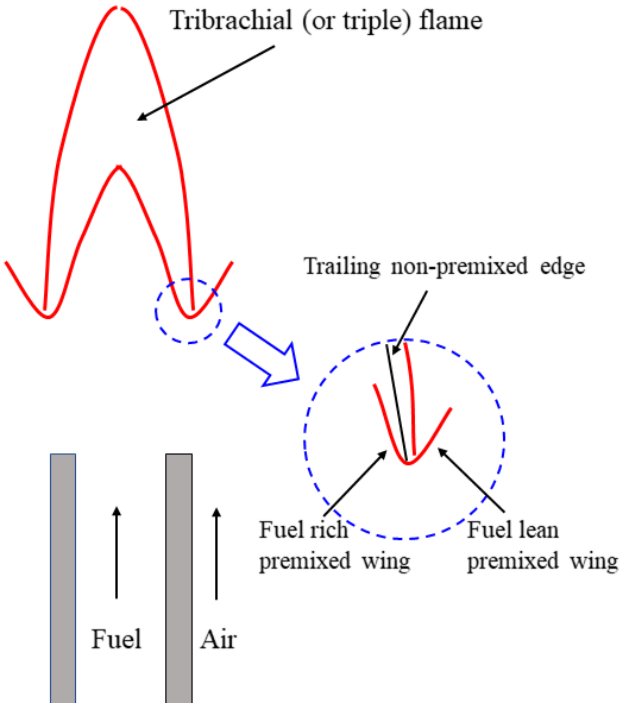

Figure 1. Schematic showing the stabilization of a laminar lifted tribrachial flame.

While in a previous experimental study of autoignited laminar lifted methane/hydrogen jet flames [24], an unusual liftoff height variation with U_0 was observed, or H_L decreases with increasing U_0 at relatively-low inlet temperatures and relatively-high hydrogen content; the decreasing H_L with U_0 does not follow the conventional autoignited laminar liftoff height behavior of $H_L \sim U_0$ [24]. It was conjectured that the unusual H_L behavior might be attributed to differential diffusion between methane and hydrogen molecules in the fuel jet. Moreover, due to the unusual characteristics of the autoignited laminar lifted methane/hydrogen jet flames, another unique feature of the flames was identified that the flame structure changes from the MILD combustion to the lifted flame with tribrachial edge with increasing U_0 although the fuel jet is not excessively diluted with an inert gas. According to previous studies of autoignited laminar lifted flames with a single component fuel such as methane and propane, the transition from tribrachial edge flame to MILD combustion was typically observed when the inlet

fuel mole fraction, $X_{F,0}$ is $O(0.01)$ [22, 28]. In the autoignition of methane/hydrogen jets in heated coflow air, however, a gradual transition from tribrachial flame to MILD combustion was observed with decreasing U_0 even though the fuel jet is not highly diluted with nitrogen ($X_{F,0} \sim O(0.1)$).

Therefore, the objective of the present study is two-fold: (1) to understand the liftoff characteristics of autoignited laminar lifted methane/hydrogen jet flames, especially the reason of the occurrence of the decreasing behavior of H_L with U_0, and (2) to elucidate the flame stabilization and structure characteristics of the autoignited laminar lifted jet flames by performing 2-D detailed numerical simulations for different inlet fuel jet conditions and hydrogen mass diffusivities. The MILD combustion featured by very faint blue flame has many advantages in reducing soot and NO_x due to its low flame temperature, and in achieving high thermal efficiency through its high reactant temperature [33, 34], and hence, it is another name of low temperature combustion (LTC) adopted in advanced IC engines. In the present study, therefore, the characteristics of autoignited laminar lifted flames with MILD combustion will also be investigated.

2. Numerical Methods

Detailed numerical simulations of autoignited laminar lifted methane/hydrogen non-premixed jet flames in heated coflow air are performed in an axisymmetric coflow burner configuration, which has been adopted in several previous experimental and numerical studies [22-28]. The following steady compressible Navier-stokes, species continuity, and energy equations are solved using laminarSMOKE [35, 36], which is an open-source code based on OpenFOAM [37] for simulations of multi-dimensional compressible laminar reacting flows with skeletal/detailed chemical mechanisms:

$$\nabla(\rho\mathbf{v}) = 0,$$

$$\nabla(\rho\mathbf{v}\mathbf{v} + p\mathbf{I}) = \nabla\boldsymbol{\tau} + \rho\mathbf{g},$$

$$\nabla(\rho Y_k\mathbf{v}) = -\nabla(\rho Y_k\boldsymbol{V_k}) + \dot{\Omega}_k,$$

$$\rho C_p\mathbf{v}\nabla T = -\nabla\mathbf{q} - \rho\sum_{k=1}^{NC} C_{p,k}Y_k\boldsymbol{V_k} - \sum_{k=1}^{NC} h_k\dot{\Omega}_k,$$

where ρ is the density, $\mathbf{v}$ the gas mixture velocity, $\boldsymbol{\tau}$ the stress tensor, $\mathbf{g}$ the gravity vector, Y_k the mass fraction of species k, $\boldsymbol{V_k}$ the diffusion velocity of species k, $\dot{\Omega}_k$ the net production rate of species k, C_p the specific heat of mixture at constant pressure, $\mathbf{q}$ the heat flux, and h_k the local enthalpy of species k. The mass and momentum conservation equations are solved by SIMPLE algorithm in steady laminarSMOKE solver, and transport and reaction terms are decoupled in the species and energy conservation equation to remedy the stiffness issue between the transport and reaction terms. For a detailed description of laminarSMOKE solver, readers are referred to [35, 36]. A skeletal 30-species of methane/air kinetic mechanism [38] based GRI-Mech 3.0 is adopted for the present simulations.

Two dimensional coflow burner adopted in the present study is schematically shown in figure 2. The main domain size is 6.65 cm × 50 cm in the radial r- and the axial z-directions. The diameter of fuel jet is 1.88 mm with 0.5 mm nozzle thickness. 3 cm of fuel nozzle is attached to the main domain, and 1 cm of fuel nozzle is protruded to the coflow air inlet to consider the wall effect of the fuel nozzle on the flow. Note that the configuration of the computational domain is identical to those of previous experiments and simulations [22-24, 28]. In the r- direction, a grid space of 0.1 mm is uniformly applied for $0 \le r \le 3$ cm to resolve the flame structure effectively, and stretched grids are distributed to the remaining domain. In the z- direction, uniform 0.1 mm grids are equally applied. Grid convergence study is carried out for the $U_0 = 15$ m/s case of low temperature high hydrogen (LTHH) condition, which detail condition will be described in the next section, with varying the grid size from 0.2 mm (coarser) to 0.05 mm (finer). Figure 3 is the result of grid convergence study, showing that the current mesh size

of 0.1 mm (normal) has almost no discrepancy with the result with mesh size of 0.05 mm (denser). Therefore, the current mesh size of 0.1 mm can be considered as fine enough size to capture the physical phenomena of the autoignited laminar lifted methane/hydrogen jet flame in heated coflow.

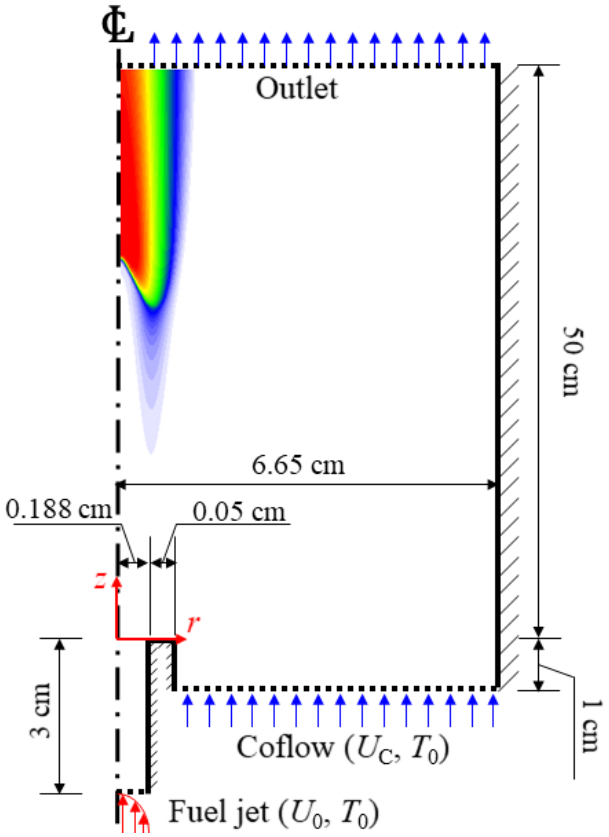

Figure 2. Schematic of the computational configuration for the present simulations of autoignited laminar lifted methane/hydrogen jet flames in heated coflow.

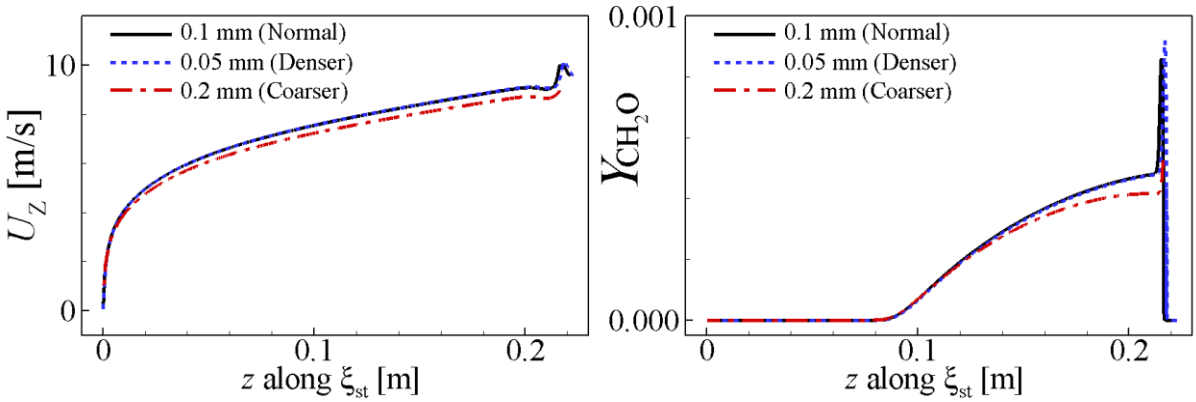

Figure 3. Grid convergence study on the velocity (left), and mass fraction of CH_2O (right) along the stoichiometric mixture fraction isoline, ξ_{st}, for the U_0 = 15 m/s of LTHH condition.

All the boundary conditions are consistent with the experimental conditions. No-slip and adiabatic boundary conditions are applied for all wall boundaries, and symmetric boundary condition is used for $r = 0$. Fully developed pipe flow condition is applied for the fuel jet inlet with the mean flow velocity of U_0, and coflow velocity, U_C, is fixed to be 1.1 m/s. Fixed value of inlet temperature T_0 is specified for both fuel and air inlets. For the outlet, zero-gradient outflow boundary conditions are used. Pressure boundary condition at inlet and outlet are zero-gradient and atmospheric, respectively. Methane/hydrogen fuel jet is diluted with nitrogen such that the fuel mole fraction at the inlet, $X_{F,0}$, is 0.2.

3. Overall characteristics of the lifted flame

In the previous experiments of lifted flame with methane/hydrogen mixtures [24], the decreasing H_L behavior with increasing U_0 (i.e., $H_L \sim 1/U_0$) occurs when T_0 is relatively-low ($860 < T_0 < 920$ K) and hydrogen ratio in the fuel jet, R_H is relatively high ($R_H > 0.12$). Here, R_H is defined as $\frac{X_{H_2}}{X_{CH_4}+X_{H_2}}$ where X_{CH_4} and X_{H_2} represent the mole fraction of methane and hydrogen, respectively. On the other hand, H_L can be proportional to U_0 (i.e., $H_L \sim U_0$) under relatively-high T_0 and low R_H. To numerically elucidate the two different H_L variation trends in methane/hydrogen mixtures, we chose two different T_0 and R_H inlet conditions through several simulation tests. One is relatively-high temperature (T_0 = 1000 K) and low hydrogen ratio (R_H = 0.08), and the other is relatively-low temperature (T_0 = 950 K) and high hydrogen ratio (R_H = 0.3). The above two conditions are denoted hereafter as high temperature low hydrogen (HTLH) condition, and low temperature high hydrogen (LTHH) condition, respectively. It is noted that T_0 in the present simulations are greater than those in experiments [24], which is probably attributed to uncertainties in the chemical mechanism and transport data and/or experiments. This issue has been reported in the previous numerical studies [26, 28].

3.1. Autoignited laminar lifted flame under HTLH condition

Figure 4a shows temperature and OH isocontours of autoignited methane/hydrogen lifted flame with HTLH condition (i.e., T_0 = 1000 K and R_H = 0.08) as a function of U_0. The dashed and dash-dotted lines represent the mixture fraction isoline passing through the flamebase, ξ_{fb}, and the stoichiometric mixture fraction isoline, ξ_{st}(=0.330), respectively. It is readily observed that H_L increases with the increase of U_0 at this condition. The lifted flame comes to be attached to the fuel nozzle when U_0 = 10 m/s or below, which results are qualitatively consistent with the previous experimental observation [24]. Flamebase is defined as the most upstream point of $Y_{OH} = 2.3 \times 10^{-4}$ isoline, which approximately corresponds to the location of maximum heat release rate. $Y_{OH} = 2.3 \times 10^{-4}$ isoline also represents approximately 5% of its maximum increase in the domain, which is consistent with definitions used in previous studies. [20, 21]. Liftoff height H_L is the axial distance between the fuel nozzle exit to the flamebase.

Note that flamebase is shifted to the leaner side from the stoichiometry isoline, which is consistent with the previous studies of laminar/turbulent lifted flames in heated coflows [20, 21, 28]. The shifting of the flamebase to the highly-lean mixture ($\xi_{fb} < 0.1$) implies that the stabilization mechanism of autoignited laminar lifted flames would be different from that of non-autoignited laminar lifted flames in which the flamebase coincides with a point of the stoichiometric mixture line where the edge flame

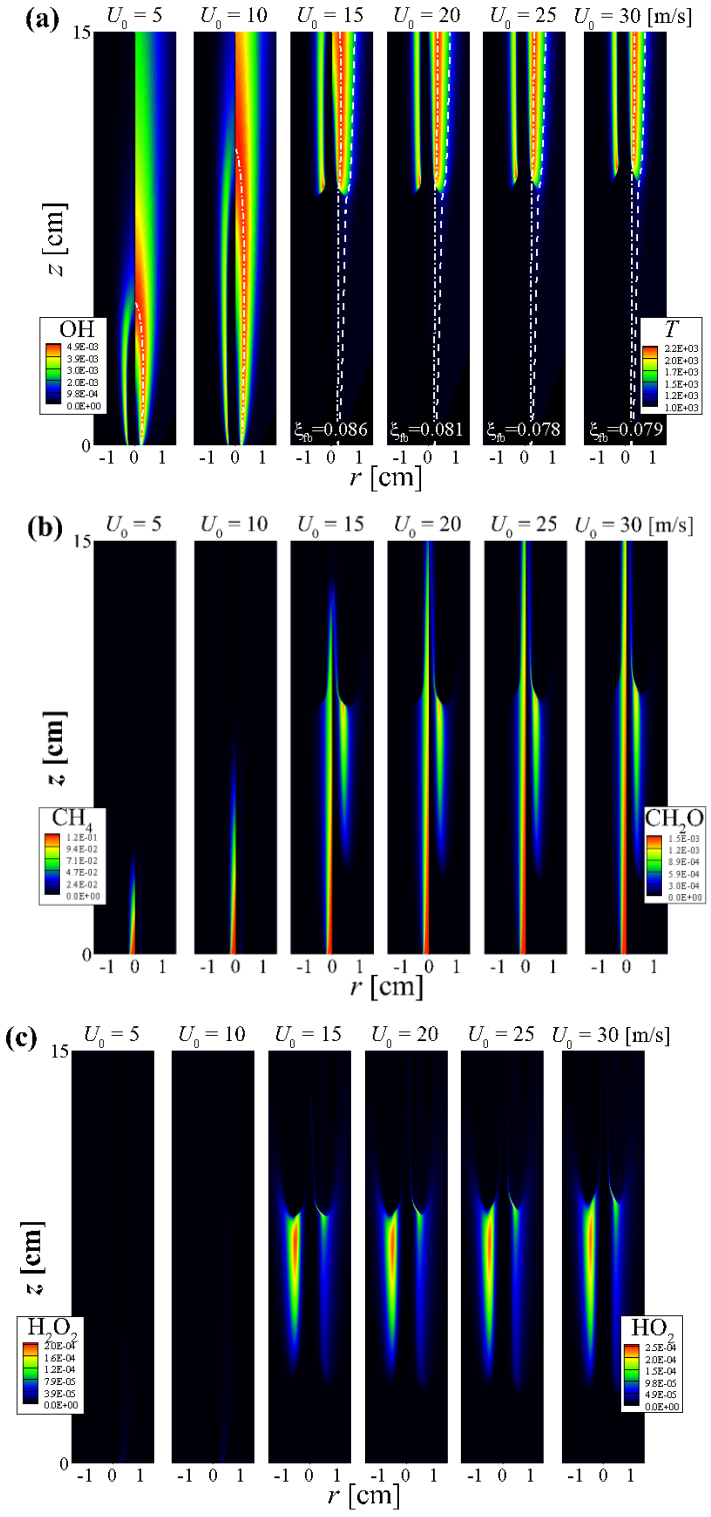

Figure 4. Isocontours of (a) T (right half), and mass fraction of OH (left half), (b) CH_2O (right half) and CH_4 (left half), and (c) HO_2 (right half) and H_2O_2 (left half) for autoignited laminar lifted methane/hydrogen jet flames under HTLH condition (T_0 = 1000 K, R_H = 0.08). The dashed and dash-dotted lines represent the mixture fraction isoline which passes through the flamebase, ξ_{fb}, and stoichiometric mixture fraction isoline, ξ_{st}(=0.330), respectively.

propagation speed balances local flow velocity [31, 32, 39, 40]. Although the lifted flame is stabilized at the fuel-lean mixture, the maximum temperature and mass fraction of OH occur following the stoichiometric mixture line in the region downstream of the flamebase, similar to previous numerical results [20, 21, 26, 28]. A detailed analysis of the flame stabilization of autoignited laminar lifted methane/hydrogen jet flames will be made in the next section.

Figure 4b and 4c show the isocontours of several species such as CH_4, HO_2, H_2O_2, and CH_2O. CH_4 is one of the main fuels consumed in the present simulations, and its concentration continuously decreases as the flow moves to the downstream because not only CH_4 is radially diffused out from the fuel jet but also CH_4 is consumed to generate the intermediate species such as CH_3 or CH_2O. In the autoignition of various kinds of hydrocarbon fuels, CH_2O, HO_2, and H_2O_2 are known to be key intermediate species during the early stage of autoignition process since they feature that their concentrations are their peaks before autoignition occurs [21, 41, 42]. As such, they are regarded as the precursors of autoignition. It is readily observed from the Fig. 4b and 4c that these intermediate species attain their maximum values at the upstream of flame region, which implies that autoignition would be predominant in the stabilization of the lifted flame [20, 21, 28].

Overall characteristics of the autoignited laminar lifted flame under HTLH condition is summarized in Figure 5 which shows H_L and $(T_{max}\text{-}T_0)/T_{ig}$ variations with the different U_0, where T_{max} is the maximum flame temperature in the domain, and T_{ig} the minimum temperature for autoignition of the stoichiometric mixture based on the inlet conditions. We determine T_{ig} under HTLH condition by considering that an autoignition can occur within the computational domain if ignition delay at $T = T_{ig}$ is less than one-jet flow-through time of the coflow air. Under the HTLH condition, T_{ig} is approximately 950 K from several 0-D ignition delay calculations by using CHEMKIN software [43]. The role of $(T_{max}-T_0)/T_{ig}$ in Fig. 5 is to identify the combustion mode of the lifted flames between the lifted flame with tribrachial edge and lifted flame with MILD combustion [22, 33, 34]. The former occurs when $(T_{max}-T_0)/T_{ig} > 1$, and the latter occurs when $(T_{max}-T_0)/T_{ig} < 1$ and $T_0 > T_{ig}$ are both satisfied [22, 28, 34]. It is readily observed from Fig.5 that $(T_{max}-T_0)/T_{ig}$ is above unity for all U_0, which indicates that only lifted flame with tribrachial edge occurs under the HTLH condition.

3.2. Autoignited laminar lifted flame under LTHH condition

Figure 6 shows temperature and mass fraction of OH, CH_4, CH_2O, HO_2, and H_2O_2 isocontours of autoignited methane/hydrogen lifted flame with LTHH condition with varying U_0 from 3.5 to 25 m/s. In contrast to HTLH condition, it is readily observed from the figure that H_L decreases with the increase of U_0, which represents the unusual characteristics of methane/hydrogen jet flame. Furthermore, we cannot observe any nozzle attached flames within the entire range of fuel jet velocity. As mentioned

above, this unusual H_L behavior has been experimentally observed in [24].

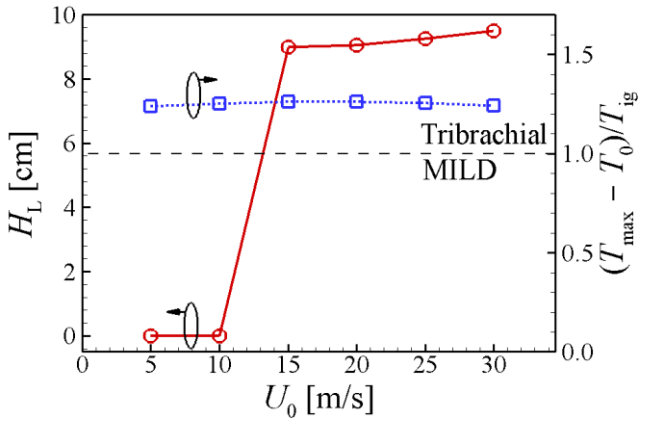

Figure 5. H_L and $(T_{max}-T_0)/T_{ig}$ with different U_0 for autoignited laminar methane/hydrogen jet flames under HTLH condition (T_0 = 1000 K, R_H = 0.08).

To understand the characteristics of lifted flame more quantitatively, H_L and $(T_{max}-T_0)/T_{ig}$ for all the cases are summarized in figure 7. Here, T_{ig} is estimated approximately 890 K under the LTHH condition. Several points are noted from the figure 6 and 7. First, the $(T_{max}-T_0)/T_{ig}$ varies significantly for cases with $U_0 \leq$ 10 m/s as U_0 decreases and the overall flame structure changes from a lifted flame with tribrachial edge to a lifted flame with MILD combustion, say, at $U_0 \leq$ 5 m/s. Furthermore, stoichiometry isoline shown in figure 6 is lower than the flame region at U_0 =10 m/s or below, which represents that overall flame structure is governed by lean-mixtures at these U_0 cases. Based on the temperature and mixture fraction information, we classify the three different flame regimes as a function of U_0 under the HTHH condition: (1) lifted flame with tribrachial edge for $(T_{max}-T_0)/T_{ig}$ is above unity (hereinafter denoted by the tribrachial edge flame regime; U_0 = 15 ~ 25 m/s), (2) lifted flame with MILD combustion for the sufficiently low $(T_{max}-T_0)/T_{ig}$ (denoted by MILD combustion regime; U_0 = 3.5 ~ 5 m/s), and (3) transition regime between the lifted flame with tribrachial edge and MILD combustion regimes (denoted by transition regimes; U_0 = 8 ~ 10 m/s). Second, figure 6(b) and 6(c) show that intermediate species such as CH_2O, HO_2, and H_2O_2 are predominant at the upstream of flamebase for all U_0 cases, which indicates that the autoignition affects the stabilization of the lifted flames. Third, H_L decreasing tendency with the U_0 increasing is different with the tribrachial and MILD combustion regime; H_L significantly changes with the U_0 variations in MILD combustion regime where H_L variation is marginally observed in tribrachial regime. From these results, we can conjecture that the unusual decreasing behavior of H_L under LTHH condition would be attributed to the characteristics of autoignition and MILD combustion, which depends on the hydrogen content in the fuel jet. The details will be further discussed later.

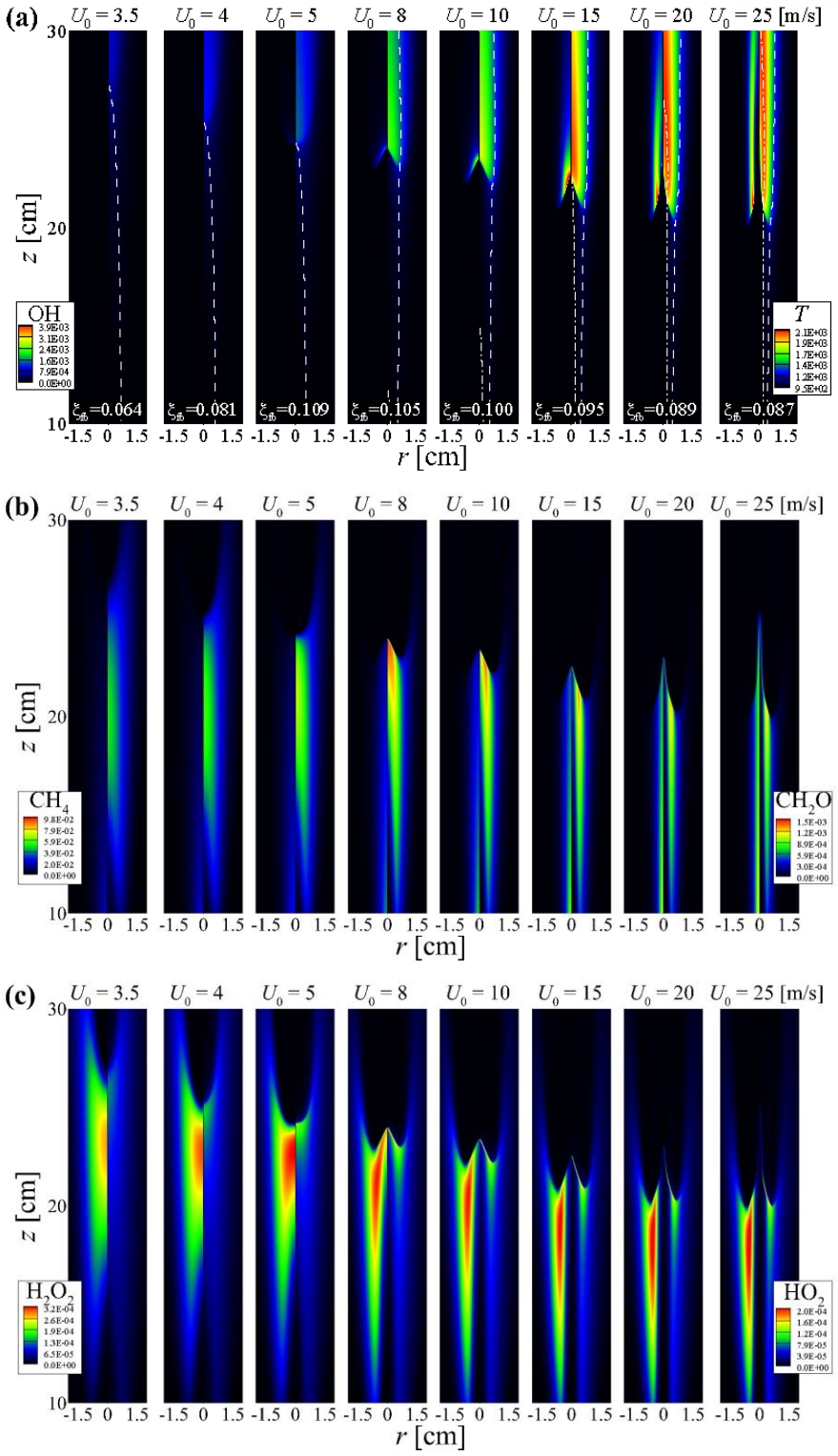

Figure 6. Isocontours of (a) T (right half), and mass fraction of OH (left half), (b) CH_2O (right half) and CH_4 (left half), and (c) HO_2 (right half) and H_2O_2 (left half) for autoignited laminar lifted methane/hydrogen jet flames under LTHH condition (T_0 = 950 K, R_H = 0.3). The dashed and dash-dotted lines represent the mixture fraction isoline which passes through the flamebase, ξ_{fb}, and stoichiometric mixture fraction isoline, ξ_{st}(=0.368), respectively.

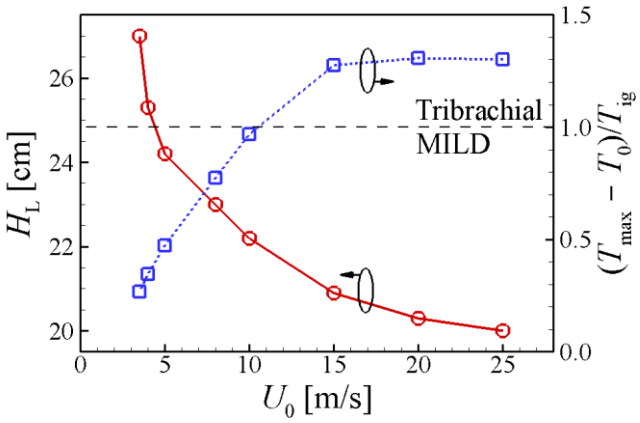

Figure 7. H_L and $(T_{max}-T_0)/T_{ig}$ with different U_0 for autoignited laminar methane/hydrogen jet flames under LTHH condition (T_0 = 950 K, R_H = 0.3).

As in the HTLH regime, we determine flamebase under LTHH condition as the most upstream point of $Y_{OH} = 2.0 \times 10^{-4}$ isoline which is approximately 5% of maximum value in the domain. However, flamebase in MILD combustion regime cannot be define with the above definition because the overall flame structure in MILD combustion fails to exhibit the tribrachial edge and maximum Y_{OH} is below 2.0×10^{-4}. To clarify the precise flamebase location in MILD combustion, therefore, we adopt Chemical Explosive Mode Analysis (CEMA) and determine the flamebase as the most upstream location of $\mathrm{Re}(\lambda_{exp}) = 0$ isoline, where λ_{exp} is an eigenvalues of the Jacobian of the chemical source term [9, 14, 44-47]. Since a mixture with $\mathrm{Re}(\lambda_{exp}) > 0$ means that the mixture is self-ignitable, while a mixture with $\mathrm{Re}(\lambda_{exp}) < 0$ is already burnt or non-ignitable. The isoline of $\lambda_{exp} = 0$ therefore denotes the boundary between the non-explosive and explosive regions, thus it can be applied to distinguish the flamebase, especially for the lean premixed mixtures. To validate the such flamebase definition, the flamebase defined by $Y_{OH} = 2.0 \times 10^{-4}$ and $\lambda_{exp} = 0$ is compared for the tribrachial edge flame, resulting in the nearly identical flamebase location between two definitions as shown in figure 8. It is noted that both isolines are proximate to the location where the heat release rate is at maximum in the domain, and maximum Y_{OH} is lower than 2.0×10^{-4} for MILD combustion case (i.e., U_0 = 4 m/s).

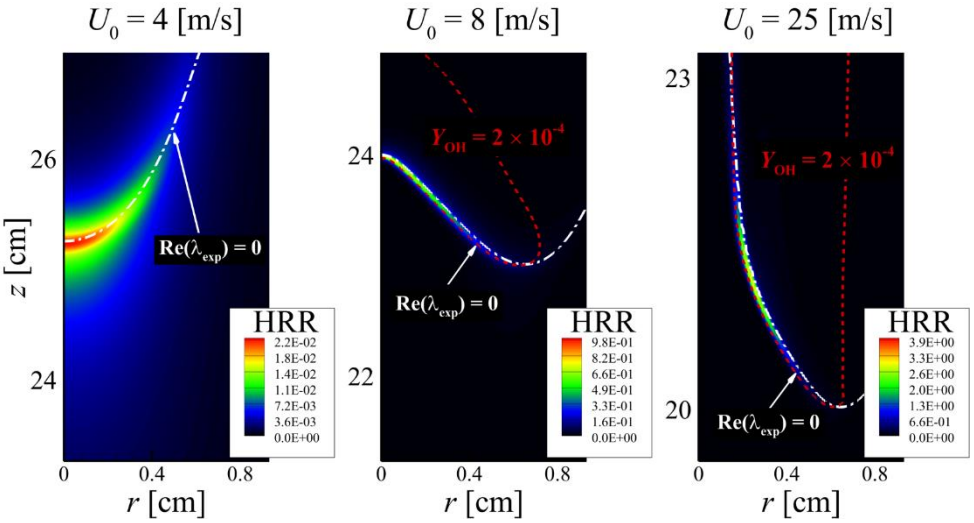

Figure 8. Isocontours of heat release rate (J/mm^{3}s) for autoignited laminar lifted methane/hydrogen jet flames with U_0 = 4, 8, and 25 m/s under the LTHH condition. Red dash line and white dash-dotted line represent the Y_{OH} = 2.0 × 10^{-4} and Re(λ_{exp}) = 0 isolines, respectively.

4. Hydrogen effect on H_L and ignition

As mentioned above, Choi et al. [24] conjectured that the unusual decreasing H_L behavior with increasing U_0 would be attributed to the disparity between methane and hydrogen mass diffusivities. This hypothesis was based on an observation that H_L varies significantly at relatively-low jet velocities which provide enough flow time to amplify the differential diffusion effect on the stabilization of the laminar lifted jet flames. To verify whether the high diffusive nature of hydrogen molecules induces the unusual decreasing H_L tendency or not, we performed additional numerical simulations by artificially changing the mass diffusivity of hydrogen molecule, D_{H_2}, to that of methane.

4.1. Effect of D_{H_2} on H_L

Figure 9 shows the temperature and mass fraction of OH, CH_4, CH_2O, HO_2, and H_2O_2 isocontours of autoignited laminar lifted methane/hydrogen jet flames with modified D_{H_2}. Contrary to the cases with normal D_{H_2}, H_L increases with increasing U_0, which clearly shows the effect of D_{H_2} on the liftoff characteristics of the lifted methane/hydrogen jet flames. It is also of interest to note that CH_2O and H_2O_2 also develop upstream of the flamebase, similar to those in the cases with normal D_{H_2}. However, their developing regions especially in the MILD combustion regime are confined within relatively-small area upstream of the flamebase compared to those in the normal cases. This is also attributed to the disparity between the normal and modified D_{H_2} which consequently changes the ignition characteristics of the methane/hydrogen fuel jet. It is also readily observed that the stoichiometric contour height is always smaller than the flamebase and the lifted flames are stabilized at fuel-lean mixtures (i.e., $\xi_{fb} < \xi_{st}$), implying that the lifted flames are controlled by autoignition of lean mixtures.

To quantitatively compare the characteristics of the lifted jet flames with normal and modified D_{H_2} under the LTHH condition, $(T_{max}-T_0)/T_{ig}$ together with H_L is shown in Fig. 10. Two points are to be noted from the figure. First, while H_L shows the opposite trends with increasing U_0 for cases with normal and modified D_{H_2}, $(T_{max}-T_0)/T_{ig}$ value increases monotonically from the MILD combustion regime to the transition regime to the tribrachial edge flame regime. These results confirm that the decreasing H_L behavior of the lifted methane/hydrogen jet flames under the LTHH condition is mainly caused by the large mass diffusivity of hydrogen molecules while the combustion mode of the lifted flames represented by $(T_{max}-T_0)/T_{ig}$ does not change much with D_{H_2}.

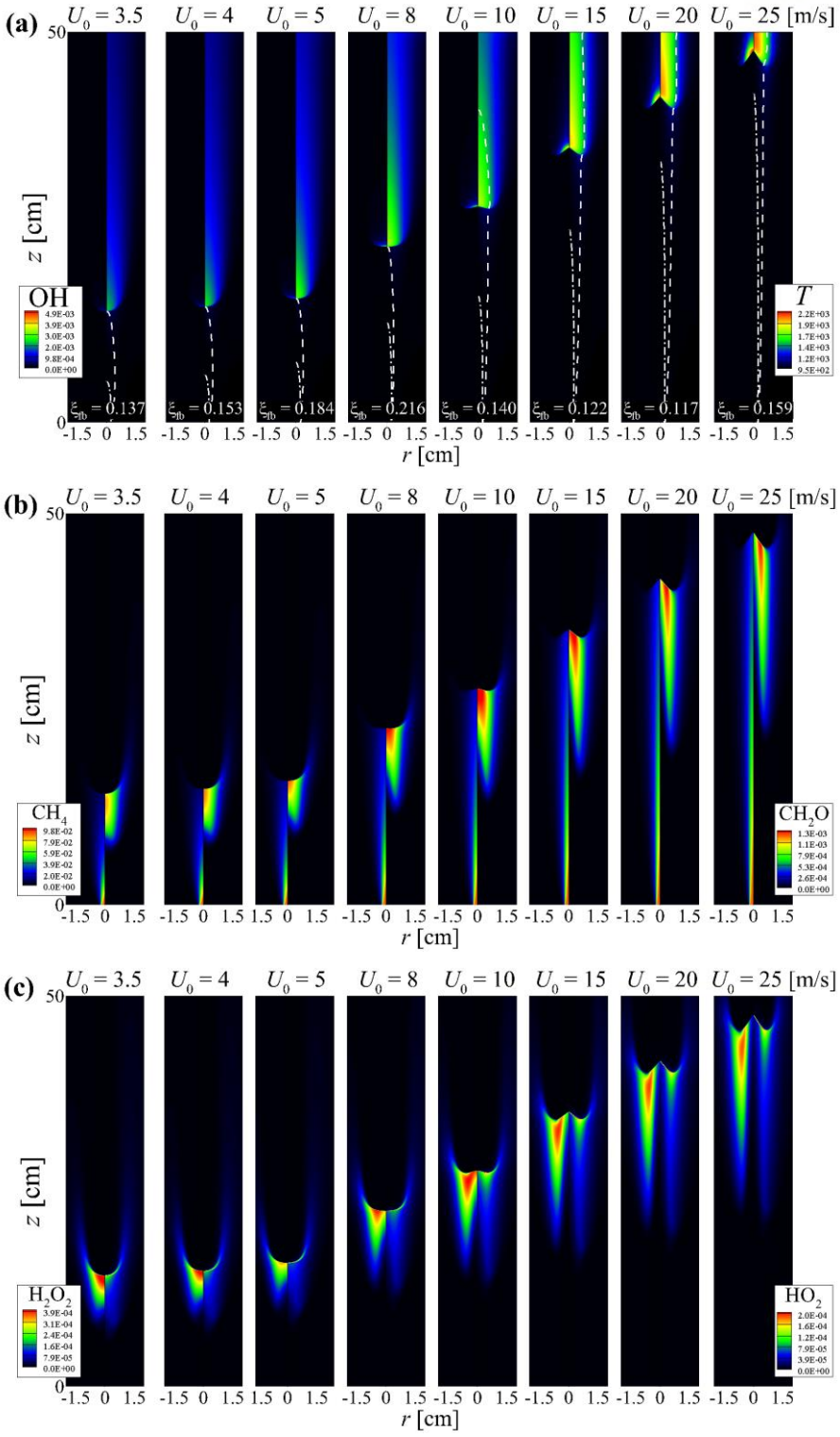

Figure 9. Isocontours of (a) T (right half), and mass fraction of OH (left half), (b) CH_2O (right half) and CH_4 (left half), and (c) HO_2 (right half) and H_2O_2 (left half) for autoignited laminar lifted methane/hydrogen jet flames with modified hydrogen's diffusivity (T_0 = 950 K, R_H = 0.3). The dashed and dash-dotted lines represent the mixture fraction isoline which passes through the flamebase, ξ_{fb}, and stoichiometric mixture fraction isoline, ξ_{st}(=0.368), respectively.

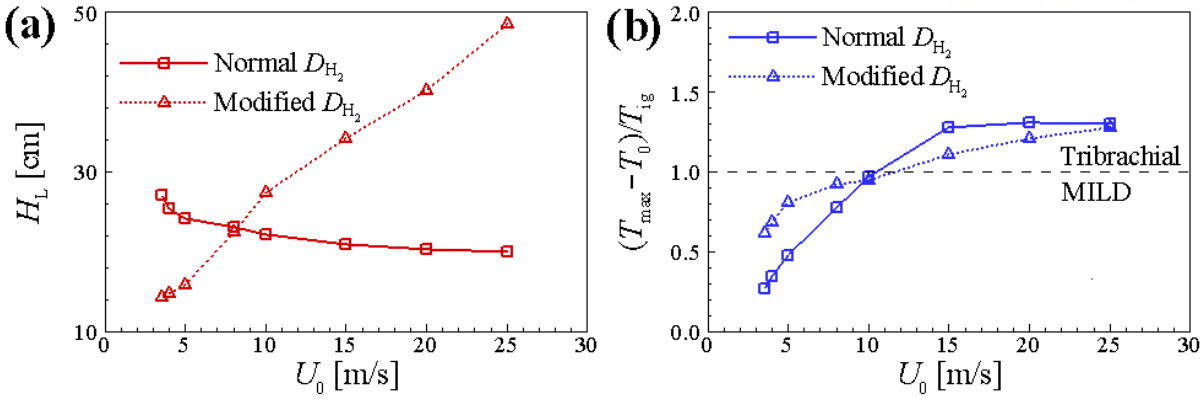

Figure 10. The variation of (a) H_L and (b) $(T_{max}-T_0)/T_{ig}$ for various fuel jet velocities with normal and modified H_2 diffusivity under the LTHH condition (T_0 = 950 K, R_H = 0.3).

To further identify how the large D_{H_2} affects the mixture condition at the flamebase and resultant autoignition characteristics, we examine the ignition delay, $\tau_{ig,fb}$, and hydrogen ratio, $R_{H,fb}$, based on the mixture condition at the flamebase as shown in Figure 11. $\tau_{ig,fb}$ is the ignition delay of the mixture at the flamebase of which species components are converted to the original fuel and oxidizer at the inlets. So, it can be evaluated as follows. We first convert the mixture at the flamebase to unburned components of CH_4, H_2, O_2, and N_2 by using the element conservation law. Then, we evaluate the ignition delay of the unburned mixture, $\tau_{ig,fb}$, assuming that it is originally located at the inlet, or its temperature is T_0. In the same way, is calculated from the unburned fuel components.

It is readily observed from Figure 11 that $R_{H,fb}$ increases from nearly zero to 0.41 with increasing U_0 for cases with normal D_{H_2} while the corresponding $\tau_{ig,fb}$ decreases with increasing U_0. Especially, $\tau_{ig,fb}$ exhibits very large value at the MILD combustion regime due to longer ignition delays of methane/hydrogen/air mixtures with small R_H compared to those with large R_H. On the contrary, the variation of $R_{H,fb}$ for cases with modified D_{H_2} is marginal and hence, the corresponding $\tau_{ig,fb}$ remains nearly the same for all cases with different U_0. Therefore, the effect of ignition on the liftoff height variation remains the same for all cases with modified D_{H_2} and hence, H_L increases with increasing U_0.

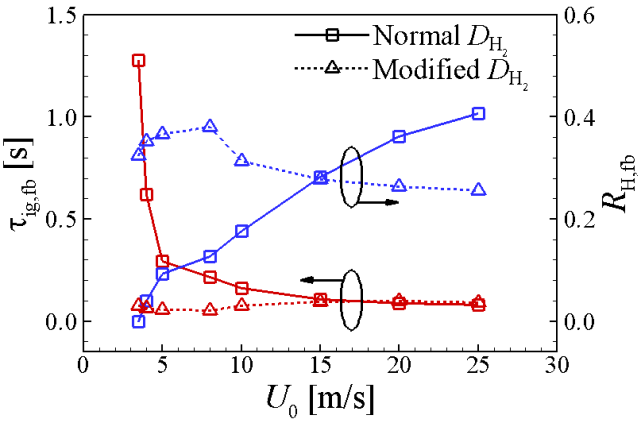

Figure 11. Ignition delay, $\tau_{ig,fb}$, and hydrogen ratio, $R_{H,fb}$, based on the mixture condition at the flamebase as a function of fuel jet velocity U_0 under the LTHH condition (T_0 = 950 K and R_H = 0.30).

As shown in Fig. 6, the radial location of the flamebase moves from the center for the MILD combustion regime to radially-outer position for the tribrachial edge flame regime. For the tribrachial edge flame regime, therefore, more hydrogen molecules from the fuel jet diffuse into the flamebase, resulting in high $R_{H,fb}$. For the MILD combustion regime, however, hydrogen molecules diffuse out from the center and thus, only methane molecules are left at the flamebase especially for very low U_0. As a result, the original unburned mixture with high $R_{H,fb}$ auto-ignites faster than that with low $R_{H,fb}$, which is consistent with previous studies of the hydrogen addition effect on methane oxidation [48, 49]. These autoignition characteristics imply that H_L of the lifted methane/hydrogen jet flames under the LTHH condition would decrease with increasing U_0, provided that their stabilization mechanism at the flamebase is autoignition.

It is also of interest to note that the MILD combustion occurs nearly regardless of $R_{H,fb}$ when the fuel jet velocity is low enough. At relatively-low U_0, the fuel molecules in the fuel jet can have enough time to diffuse out and thus, the fuel mole fraction decreases significantly even at the center of the fuel jet, resulting in fuel-lean mixture at the flamebase. The ignition delay at the center becomes the shortest and the MILD combustion features a flat or "U"-shaped structure depending on the axial velocity profile. In addition, small D_{H_2} makes the mixture at the center relatively fuel-richer than that with large D_{H_2} and hence, for the MILD combustion regime, H_L with modified D_{H_2} become shorter than those with normal D_{H_2}, and vice versa for the tribrachial edge flame regime as shown in Fig.10. Thus, it is reasonable that the liftoff heights with normal and modified D_{H_2} intersect nearly at the boundary between the tribrachial edge flame and the MILD combustion regimes or at the transition regime featured by $(T_{max}-T_0)/T_{ig} \approx 1$.

To verify how the lifted flames are stabilized under the LTHH condition, we performed Damköhler

number analysis along the mixture fraction isoline passing through the flamebase, ξ_{fb}. Damköhler number, *Da*, is defined as τ_{flow}/τ_{ig} which is the ratio of characteristic flow time τ_{flow} to characteristic ignition delay time τ_{ig}. Damköhler number analysis is performed by evaluating *Da* at every point of ξ_{fb} isoline, which delineates white dashed line in the Fig.6. ξ_{fb} is adopted as the reference line for the present Damköhler number analysis because tracing the mixture fraction isoline in 2-D spatial domain is known as to contain the time history of mixture's autoignition process [29, 30]. The characteristic flow time, τ_{flow}, is defined as the time required for a fluid particle to reach the flamebase from a specific point on the ξ_{fb}, and the characteristic ignition delay time, τ_{ig}, is obtained by calculating the 0-D ignition delay time at each point. Damköhler number analysis could be interpreted as the following ways. If *Da* < 1 at the all points upstream of flamebase, it indicates that the time for the mixtures to autoignite (τ_{ig}) takes longer than the time to arrive the flamebase from the point (τ_{flow}). Thus, *Da* < 1 at the upstream implies that the mixtures would reach the flamebase before it is fully consumed by autoignition, then the flamebase may be stabilized by the flame propagation rather than autoignition. When *Da* > 1 region exists on the upstream of flamebase, on the other hand, autoignition would play a dominant role of the flame stabilization since τ_{ig} is shorter than τ_{flow} at the upstream of flamebase. Damköhler number analysis in two-dimensional domain is carried out for each case in LTHH condition, and the result of U_0 = 4, 8, 25 m/s cases are shown in the Fig. 12, which represent the MILD combustion regime, transition regime, and tribrachial edge flame regime, respectively. All the other cases show the similar results with the representing cases, and are therefore not shown in this thesis.

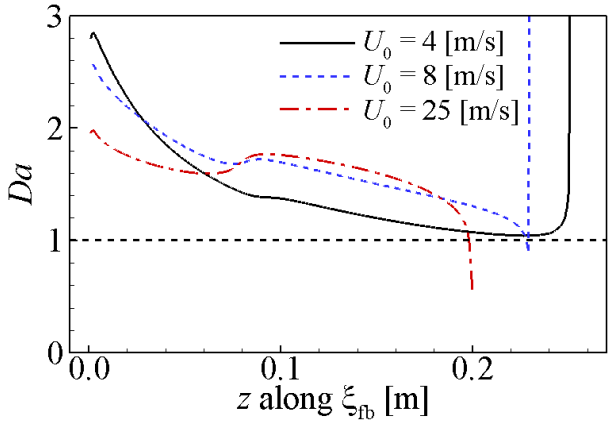

Figure 12. Damköhler number analysis along the mixture fraction isoline passing through flamebase, ξ_{fb}, for the cases of U_0 = 4, 8, 25 m/s

It is readily observed from the Fig.12 that all the cases have the regime where *Da* is above unity, implying that mixtures arriving to the flamebase are highly autoignitable ($\tau_{ig} < \tau_{flow}$). Therefore, it indirectly indicates that autoignition is important for the stabilization of flamebase for the all cases. It

is also noted that *Da* near the flamebase contains some uncertainty because both τ_{flow} and τ_{flow} near the flamebase are very low ($O(10^{-4}$ s)), such that both are highly sensitive to the small modification of flamebase definition.

To further verify the stabilization mechanism of flamebase for each case, we performed transport budget analysis along the ξ_{fb}, similar to [50-52]. In the present study, OH is adopted for the analysis since it is often used as a flame marker. Species transport equation for the mass fraction of species OH in steady state is as follows:

$$0 = -\nabla(\rho Y_{\text{OH}}\mathbf{v}) - \nabla(\rho Y_k \boldsymbol{V_k}) + \dot{\Omega}_k,$$

convection term, **C**, is represented by the first term on the right-hand side, and second and third terms in right-hand side represent the diffusion, **D**, and chemical reaction, **R**, respectively. In a steady state, **R** balances **D** in the reaction zone of normal flames while **C** is negligible. In autoignition process, however, **R** balances **C** with negligible **D**.

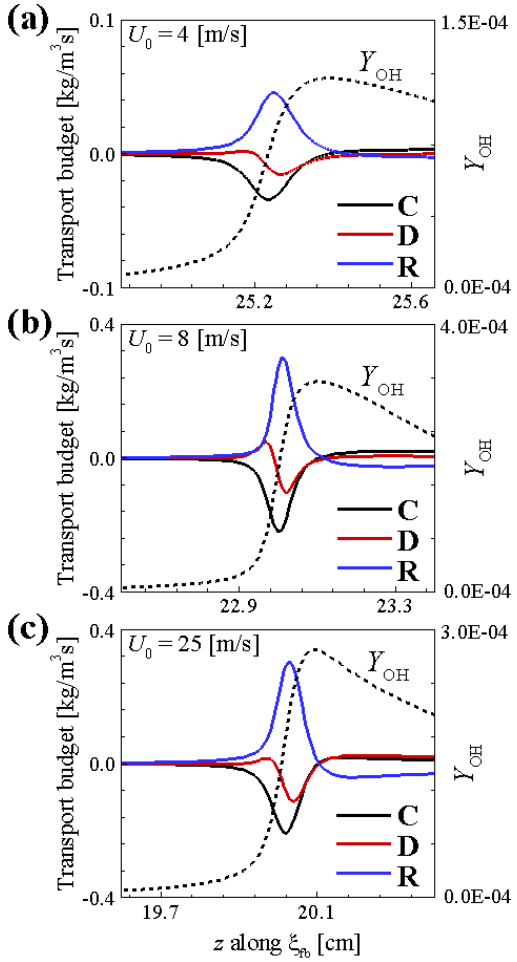

Figure 13. The profiles of convection, diffusion, and chemical reaction terms along the mixture fraction isoline passing through the flamebase, ξ_{fb}, for cases (a) $U_0 = 4$, (b) 8, and (c) 25 m/s.

Figure 13 shows the profiles of **C**, **D**, and **R** along the ξ_{fb} isoline for cases with U_0 = 4, 8, and 25 m/s under the LTHH condition, each of which represents the MILD combustion, the transition, and the tribrachial edge flame regime, respectively. It is readily observed that for all cases, **R** is mainly balanced with **C** near the flamebase or at the maximum **R** location while the contribution of **D** to the transport budget is relatively small, which implies that the lifted flames are primarily stabilized by autoignition rather than flame propagation.

4.2. Ignition characteristics: CEMA

To further elucidate the spatial ignition and flame stabilization characteristics, we performed the chemical explosive mode analysis (CEMA) of the lifted flames. CEMA has been successfully adopted to systematically identify key species and reactions for premixed/non-premixed flames and ignition/extinction processes in laminar/turbulent lifted jet flames in heated coflows [53, 54], turbulent reacting jet flames in cross flows [21, 29, 30, 44, 45], and ignition of hydrocarbon fuel/air mixtures under HCCI conditions [9, 11, 12, 14, 46, 47].

As mentioned above, the Jacobian of the chemical source term of the discretized conservation equations for a chemically-reacting system has the chemical information of local mixtures and hence, we can determine their chemical characteristics using the Jacobian [44-46]. To identify the chemical feature in CEMA, a chemical mode is defined as an eigenmode of the Jacobian, which is associated with an eigenvalue, λ_e, and a corresponding pair of the left and right eigenvectors, $\mathbf{a}_e$ and $\mathbf{b}_e$. Chemical explosive mode (CEM) is a chemical mode of which real part of eigenvalue is positive, $\mathrm{Re}(\lambda_e) > 0$.

From CEMA, the critical chemical kinetic processes occurring in the autoignited laminar lifted flames can be identified by evaluating explosive index (EI) and participation index (PI) of local mixtures. EI and PI are defined as [45-47]:

$$\mathrm{EI} = \frac{\left|\mathbf{a}_e \otimes \mathbf{b}_e^{\mathrm{T}}\right|}{\sum\left|\mathbf{a}_e \otimes \mathbf{b}_e^{\mathrm{T}}\right|},$$

$$\mathrm{PI} = \frac{\left|(\mathbf{b}_e \cdot \mathbf{S}) \otimes \mathbf{R}\right|}{\sum\left|(\mathbf{b}_e \cdot \mathbf{S}) \otimes \mathbf{R}\right|},$$

where **S** and **R** represent the stoichiometric coefficient matrix and the vector of the net rates for reactions, respectively. The symbol $\otimes$ denotes the element-wise multiplication of two vectors. EI and PI indicate the normalized contribution of each variable and reaction to a CEM, respectively, and as such, key species and reactions to ignition near the flamebase can be elucidated by evaluating EI and PI values.

Figure 14 shows the EI isocontours of several important variables for the lifted flames in three different regimes, i.e. $U_0 = 4$, 8, and 25 m/s under the LTHH condition. Heat release rate is also presented in the figure to show the flame location. Several points are to be noted from the figure. First, for all regimes, the most important EI variable upstream of the flamebase is temperature while CH_3, CH_2O, and HO_2 also contribute to the CEM further upstream of the flamebase, showing a general sequence of autoignition of methane/air mixture [55]. Second, for the MILD combustion regime (U_0 = 4 m/s), the contribution of CH_2O to the CEM is confined within a relatively-short and broad region between the fuel jet and the flamebase. However, for the tribrachial edge flame regime ($U_0 = 25$ m/s), its contribution

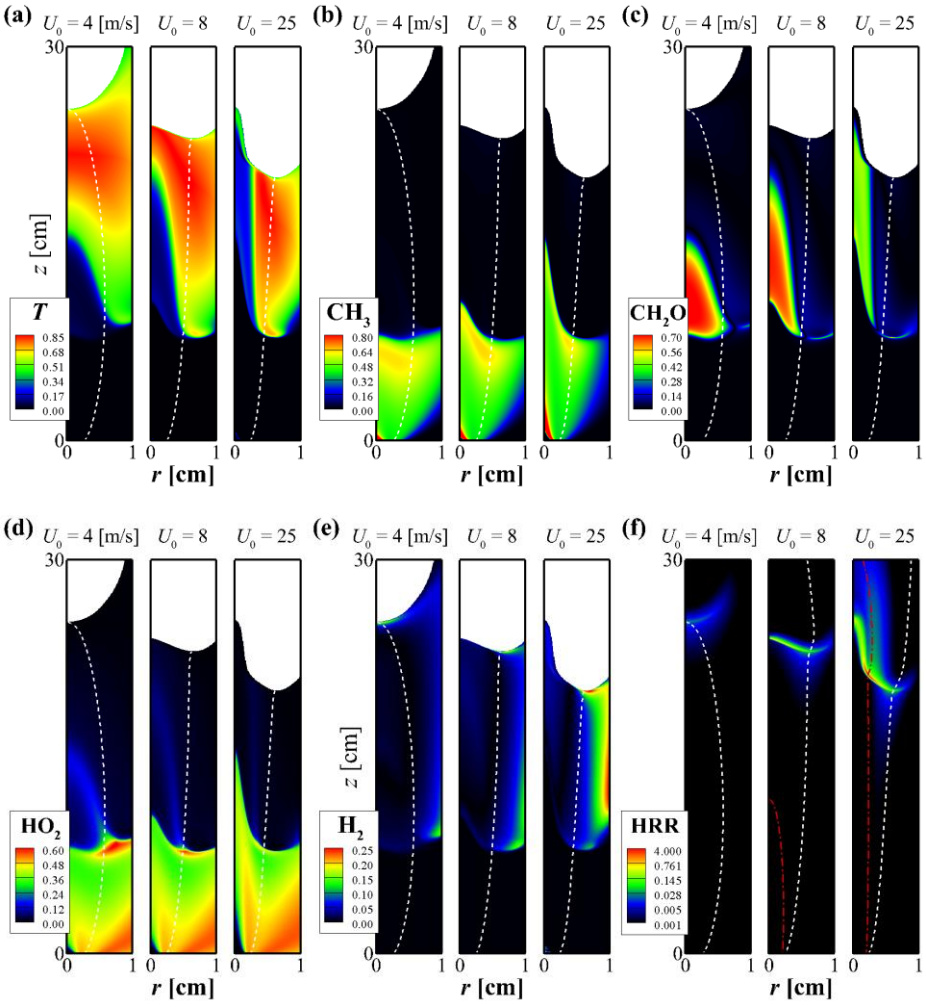

Figure 14. Isocontours of EI of (a) T, (b) CH_3, (c) CH_2O, (d) HO_2, and (e) H_2, and (f) heat release rate (J/mm^{3}s) for autoignited laminar lifted methane/hydrogen jet flames with U_0 = 4, 8, and 25 m/s under the LTHH condition. The dashed line represents the mixture fraction isoline passing through the flamebase, ξ_{fb}. The white area is intentionally added, which corresponds to $Re(\lambda_{exp}) < 0$.

area narrows and elongates till the flame. For the MILD combustion regime, both methane and hydrogen diffuse out from the fuel jet and are well mixed with oxidizer, and hence, the conversion of CH_4 to CH_3

to CH_2O is finished far upstream of the flamebase. For the tribrachial edge flame regime, however, the conversion of methane to smaller intermediate species continues till the flamebase due to large U_0. Third, for the tribrachial edge flame regime, the contribution of hydrogen to the CEM is identified the second largest next to temperature right upstream of the flamebase while its contribution is negligible for the MILD combustion regime. This result verifies that hydrogen molecules with large mass diffusivity plays a critical role in stabilizing the lifted flame in the tribrachial edge flame regime.

To further identify the chemical characteristics of the lifted flames in different regimes, the contribution of each chemical reaction to the CEM, or the PI isocontours of important reactions are shown in figure 15. Although we already had a glimpse on the chemical features of the lifted flames through the EI analysis, we can further examine which reaction affects the CEM through the PI analysis. From the figure, we can readily observe the sequential ignition of methane/air and hydrogen/air mixtures. After the H abstraction from CH_4 near the fuel nozzle as shown in Fig.15(a), the conversion of CH_3 to CH_3O/CH_2O to HCO occurs in sequence through $CH_3 + (O, HO_2) \rightarrow (CH_2O + H, CH_3O + OH)$ (R10, R111), $CH_3O + (M, O_2) \rightarrow CH_2O + (H + M, HO_2)$ (-R54, R160), and $CH_2O + (H, OH, CH_3) \rightarrow HCO + (H_2, H_2O, CH_4)$ (R55, R96, R151) as shown in Fig.15(b) and (c). The final CO conversion to CO_2 appears as the main heat release step right after the conversion of HCO to CO occurring just upstream of the flame as described in Fig.15(c) and (d).

In addition, the recombination reaction of $H + O_2 + M \rightarrow HO_2 + M$ (R31-34) competes with the chain branching reaction of $H + O_2 \rightarrow O + OH$ (R35) far upstream of the flamebase. However, R35 together with $H_2O_2 + M \rightarrow OH + OH + M$ (-R80) becomes more important than R31-34 as it comes to the flamebase. Especially, the contribution of the chain branching reaction (R35) and the hydrogen heat release reaction of $H_2 + OH \rightarrow H + H_2O$ (R79) become dominant right upstream of the flamebase for the tribrachial edge flame regime. This result confirms that the hydrogen effect on the unusual decreasing H_L behavior with increasing U_0 is attributed to the hydrogen chemistry, which is originally from the fast diffusion of hydrogen molecules from the fuel jet.

In summary, the contribution of reactions related to the hydrogen oxidation to the CEM in the tribrachial edge flame regime is relatively larger than that in the MILD combustion regime, and as such, the ignition at the flamebase for the tribrachial edge flame regime occurs faster than that for the MILD combustion regime.

It is of interest to note that from the EI isocontours of the lifted flames with modified D_{H_2} as shown in figure 16, their chemical features are found quite similar to those of the lifted flames with normal D_{H_2} in the transition regime (i.e., the case with U_0 = 8 m/s). The shapes of EIs do not change much with U_0 but their area elongates or shrink along the axial direction depending on U_0. This is because for cases with modified D_{H_2}, the hydrogen and methane oxidations occur at the same radial location with

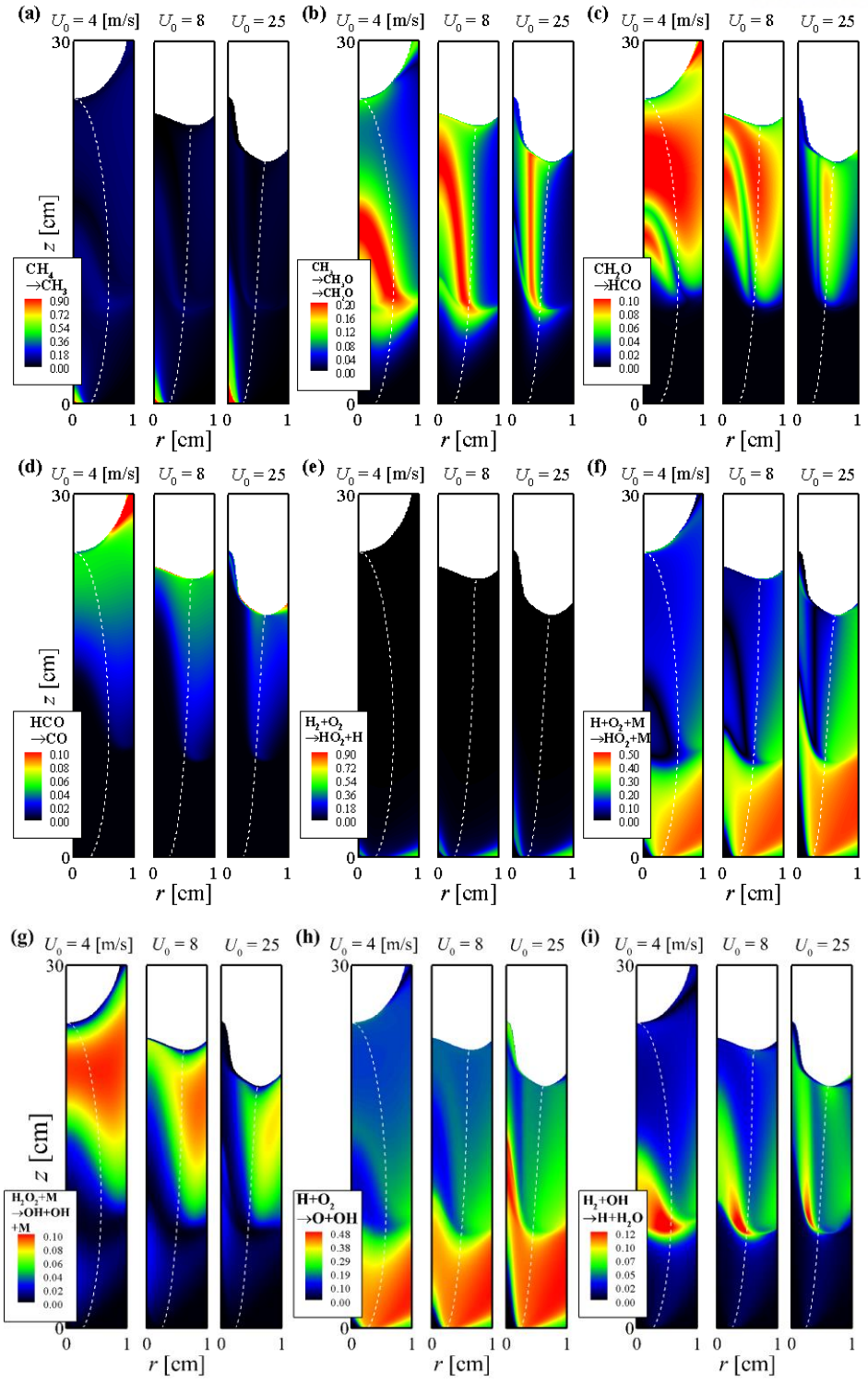

Figure 15. Isocontours of PI of (a) H-abstraction of CH_4, (b) reactions of CH_3 conversion to CH_2O and CH_3O, (c) CH_2O conversion to HCO, (d) HCO conversion to CO, (e) $H_2 + O_2 \rightarrow HO_2 + H$ (-R42), (f) H + O2 + M → HO2 + M (R31-34), (g) $H_2O_2 + M \rightarrow OH + OH + M$ (-R80), (h) $H + O_2 \rightarrow O + OH$ (R35), and (i) $H_2 + OH \rightarrow H + H_2O$ (R79) for autoignited laminar lifted methane/hydrogen jet flames for cases with U_0 = 4, 8, and 25 m/s. The white dashed line represents the mixture fraction isoline passing through the flamebase, ξ_{fb}.

different axial location due to their identical diffusivities, and hence, hydrogen only serves as an additive for advancing the autoignition of the fuel jet as demonstrated in Fig.11. Consequently, their chemical features become similar to those of the lifted flames with normal D_{H_2} in the transition regime in which the effect of large D_{H_2} on the ignition of the methane/hydrogen jet becomes minimal.

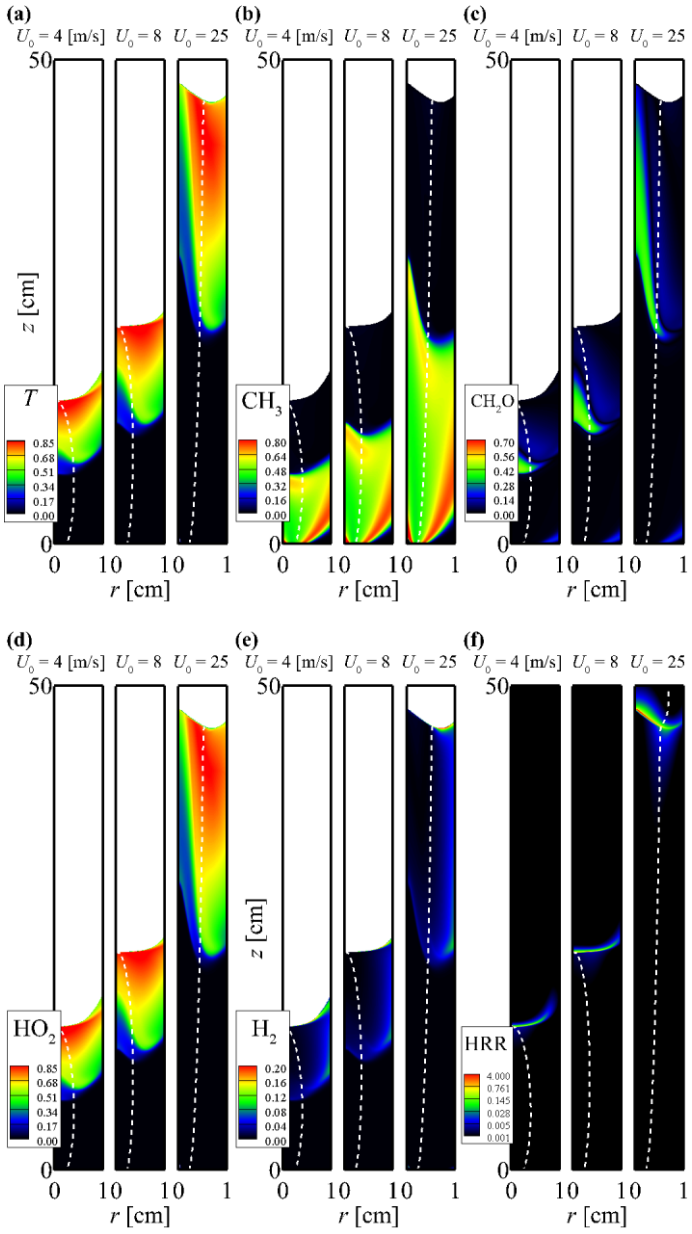

Figure 16. Isocontours of EI of (a) T, (b) CH_3, (c) CH_2O, (d) HO_2, and (e) H_2, and (f) heat release rate (J/mm^{3}s) for autoignited laminar lifted methane/hydrogen jet flames with U_0 = 4, 8, and 25 m/s with modified hydrogen's mass diffusivity. The dashed line represents the mixture fraction isoline passing through the flamebase, ξ_{fb}.

5. Liftoff height correlation

In this section, we find a liftoff height correlation for autoignited laminar lifted methane/ hydrogen jet flames under several LTHH conditions similar to those in previous experimental studies [22-24]. As demonstrated in the previous sections, the unusual H_L behavior under the LTHH condition cannot be understood with the inlet mixture conditions such as the adiabatic 0-D ignition delay of the stoichiometric inlet mixture, $\tau_{ig,st}$. As mentioned earlier, the conventional liftoff height correlation of $H_L \sim U_0\tau_{ig,st}^2$ was originally derived for autoignited lifted jet flames with a single fuel by taking into account diffusive heat loss occurring at the jet mixing layer during autoignition.

In the present study, however, a mixture of methane and hydrogen with different ignition delays and different mass diffusivities are used for the fuel such that the adiabatic 0-D ignition delay of the stoichiometric inlet mixture cannot solely represent the mixture condition at the flamebase. In other words, the differential diffusion effect of methane/hydrogen mixtures is not fully incorporated in $\tau_{ig,st}$ based on the inlet condition and hence, $H_L \sim U_0\tau_{ig,st}^2$ is no longer valid for predicting the H_L behavior under the LTHH condition. So, we devise a novel H_L correlation by noting that $\tau_{ig,fb}$ can incorporate the effect of the differential diffusion represented by $R_{H,fb}$ on the autoignition of the lifted flames as shown in Fig.11.

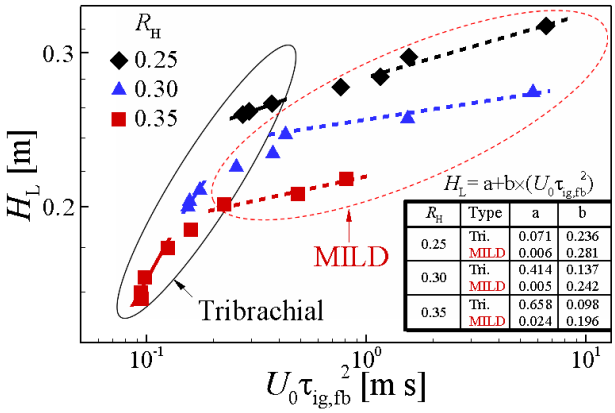

R_H	Type	a	b
0.25	Tri.	0.071	0.236
	MILD	0.006	0.281
0.30	Tri.	0.414	0.137
	MILD	0.005	0.242
0.35	Tri.	0.658	0.098
	MILD	0.024	0.196

Figure 17. Liftoff height correlation for autoignited laminar lifted methane/hydrogen jet flames under various LTHH conditions (T_0 = 950 K and R_H = 0.25, 0.30, and 0.35).

By replacing $\tau_{ig,st}$ with $\tau_{ig,fb}$ in the original H_L correlation of $H_L \sim U_0\tau_{ig,st}^2$, we obtain a novel $H_L \sim U_0\tau_{ig,fb}^2$ as shown in Figure 17. In addition to the cases under the LTHH condition (i.e., T_0 = 950 K and R_H = 0.3), other cases with different R_H of 0.25 and 0.35 are also shown in the figure. As in previous experimental studies [22-24], the tribrachial edge flame regime and the MILD combustion

regime are separated for the H_{L} correlation. It is readily observed from the figure that the new H_{L} correlation captures accurately the decreasing behavior of H_{L} with increasing U_0, verifying that the refined $\tau_{\mathrm{ig,fb}}$ represents reasonably well the ignition delay of the autoignited laminar lifted methane/hydrogen jet flames even though it cannot be obtained a priori.

It is also of interest to note that the conventional liftoff height correlation of $H_{\mathrm{L}} \sim U_0 \tau_{\mathrm{ig,st}}^2$ holds for autoignited laminar lifted jet flames with a single fuel because for these flames, $\tau_{\mathrm{ig,fb}}$ remains nearly the same for different U_0 as shown in Fig.11 and the replacement of $\tau_{\mathrm{ig,st}}$ with $\tau_{\mathrm{ig,fb}}$ may not affect the liftoff height correlation.

6. Highly MILD combustion regime ($U_0 \leq 3$ m/s)

Numerical simulation for the extremely low jet velocity regime (U_0 = 2 and 3 m/s) are carried out under LTHH condition, and heat release rate isocontour for this regime is shown in the figure 18 with U_0 = 4 and 25 m/s cases as for the reference. Although it is not shown, temperature increase of U_0 = 2 and 3 m/s cases are rarely observed (around 50 and 175 K, respectively). We hereinafter denote this regime ($U_0 \leq 3$ m/s) as "highly MILD combustion regime" because of distinct features of this regime compared to the tribrachial and MILD combustion regimes.

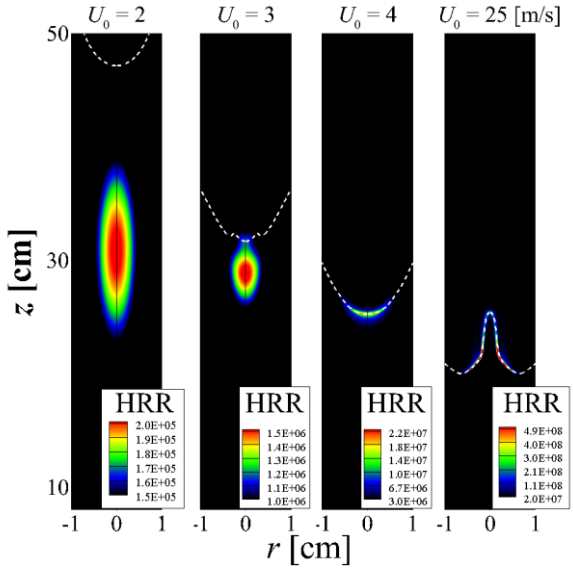

Figure 18. Heat release rate isocontours of highly MILD combustion regimes ($U_0 < 3$ m/s) with U_0 = 4 and 25 m/s cases for the reference. White dashed line represents λ_{exp} = 0 isoline.

In Highly MILD combustion regime, it is hard to define the precise flamebase location since $\mathrm{Re}(\lambda_{\mathrm{exp}}) = 0$ isoline, which was used for finding the flamebase for the MILD combustion regime, is not identical with the maximum heat release rate location. For both U_0 of 4 and 25 m/s cases, it is readily observed from Fig.18 that maximum heat release rate location is proximate to the $\mathrm{Re}(\lambda_{\mathrm{exp}}) = 0$ isoline, thus $\mathrm{Re}(\lambda_{\mathrm{exp}}) = 0$ isoline is validated to define as the flamebase position for these cases. In case of U_0 = 2 and 3 m/s, however, heat release rate is at its peak at the relatively upstream of $\mathrm{Re}(\lambda_{\mathrm{exp}}) = 0$ isoline. It indicates that unburned CH_4 and O_2 species are survived after the peak of heat release rate, and the reactants are subsequently consumed until the mixture arrives $\mathrm{Re}(\lambda_{\mathrm{exp}}) = 0$ isoline. As a consequence, it seems flame has been thickened and flamebase location is not clearly identified accordingly.

Additionally, the revised H_L relation, which was introduced by previous section, is no longer able

to predict the actual liftoff height change in highly MILD combustion regime whether flamebase is defined as the maximum heat release rate point or $\mathrm{Re}(\lambda_{\mathrm{exp}}) = 0$ isoline. It may be attributed to the uncertainty of the exact flamebase location, and autoignition characteristics of highly MILD combustion regime needs to be studied as a future work.

7. Conclusions

The characteristics of autoignited laminar lifted methane/hydrogen jet flames in heated coflow air were numerically investigated using laminarSMOKE with a 30-species skeletal chemical mechanism of methane oxidation. The detailed numerical simulations were performed for various fuel jet velocities under the HTLH and LTHH conditions. The numerical simulations captured opposite liftoff height behaviors under the HTLH and LTHH conditions, qualitatively similar to those in experiments. To identify the effect of differential diffusion on the unusual H_L behavior under the LTHH condition, additional numerical simulations with modified D_{H_2} were also carried out. The following results were obtained from the simulations together with the Damköhler number analysis, transport budget analysis and chemical explosive mode analysis (CEMA).

1. Considering the flame structure and $(T_{max}-T_0)/T_{ig}$, we categorized the autoignited laminar lifted jet flames under the LTHH condition into three different combustion regimes: the MILD combustion regime, the transition regime, and the tribrachial edge flame regime.

2. From the simulations with different D_{H_2}, it was verified that the high diffusive nature of hydrogen molecule is primarily attributed to the unusual decreasing H_L behavior with increasing U_0 under the LTHH condition.

3. Under the LTHH condition, $R_{H,fb}$ increases with increasing U_0 due to large D_{H_2}. In the MILD combustion regime, the fuel jet has enough time to diffuse out from the center, and thus, hydrogen molecules in the fuel jet diffuse out more, leading to small $R_{H,fb}$ and large $\tau_{ig,fb}$. On the other hand, in the tribrachial edge flame regime, the flamebase locates radially outside and hence, more hydrogen molecules can diffuse into the flamebase, resulting in large $R_{H,fb}$ and small $\tau_{ig,fb}$.

4. As such, $R_{H,fb}$ increases from zero to 0.41 with increasing U_0, which delays/advances autoignition in the MILD combustion regime/the tribrachial edge flame regime. As a result, H_L decreases from the MILD combustion regime to the tribrachial edge flame regime because H_L of autoignited laminar jet flames highly depends on the ignition delay rather than the fuel jet velocity.

5. From the Damköhler number analysis, all U_0 cases under the LTHH condition have the regions where Da is above unity, indicating that mixture upstream of flamebase is highly autoignitable.

6. From the species transport budget analysis, it was found that the convection and chemical reaction source terms balance each other near the flamebase with negligible diffusion term, indicating that autoignition upstream of the flamebase plays a dominant role in stabilizing the lifted flame.

7. CEMA was carried out to identify the ignition process upstream of the flamebase and to elucidate

the difference between the tribrachial edge flame and MILD combustion. In the tribrachial edge flame regime, the overall contribution of hydrogen-related reactions to the CEM becomes greater than that in the MILD combustion regime, leading to the reduction of the ignition delay at the flamebase for the tribrachial edge flame regime.

8. A novel correlation of $H_{\mathrm{L}} \sim U_0 \tau_{\mathrm{ig,st}}^2$ was proposed for the autoignited laminar lifted methane/hydrogen jet flames under the LTHH conditions by noting that $\tau_{\mathrm{ig,fb}}$ can represent the autoignition of the fuel jet more accurately than $\tau_{\mathrm{ig,st}}$. The new correlation shows good agreement with the simulation results.

9. Under the highly MILD combustion regime ($U_0 \leq 3$ m/s), flamebase is not precisely defined due the discrepancy between the maximum heat release rate and $\mathrm{Re}(\lambda_{\mathrm{exp}}) = 0$ isoline. It represents the existence of unburned reactants at the downstream of maximum heat release rate isoline, thus overall flame structure has been thickened. In this regime, a new correlation of $H_{\mathrm{L}} \sim U_0 \tau_{\mathrm{ig,st}}^2$ does not predict the actual liftoff height variations well, and further researches will be required as a further work.

References

[1] U.S. Department of Energy. Transportation energy data book. <http://cta.ornl.gov/data/index.shtml> (accessed November 2011).

[2] Shayler PJ, Wiseman MW. Improving the determination of mass fraction burnt. SAE 900351.

[3] Wang J, et al. Combustion behaviors of a direct-injection engine operating on various fractions of natural gas–hydrogen blends. Int. J Hydrogen Energy 2007 32 (2007) 3555–3564.

[4] Shayler PJ, Wiseman MW. Improving the determination of mass fraction burnt. SAE 900351.

[5] F. Ma, H. Lui, Y. Wang, Y. Li, J, Wang, S, Zhao, combustion and emission characteristics of a port-injection HCNG engine under various initial timings, International journal of hydrogen energy, 33, 2008, 816-822.

[6] E. Navarro, T. J. Leo, R. Corral, CO_2 emissions from a spark ignition engine operating on natural gas-hydrogen blends (HCNG).

[7] S. Saxena, I. D. Bedoya, Fundamental phenomena affecting low temperature combustion and HCCI engines, high load limits and strategies for extending these limits, Prog. Energy Combust. Sci. 39 (2013) 457-488.

[8] R. D. Reitz, G. Duraisamy, Review of high efficiency and clean reactivity controlled compression ignition (RCCI) combustion in internal combustion engines, Prog. Energy Combust. Sci. 46 (2015) 12-71.

[9] C. S. Yoo, T. Lu, J. H. Chen, C. K. Law, Direct numerical simulations of ignition of a lean n-heptane/air mixture with temperature inhomogeneities at constant volume: Parametric study, Combust. Flame 158 (2011) 1727-1741.

[10] C. S. Yoo, Z. Luo, T. Lu, H. Kim, J. H. Chen, A DNS study of ignition characteristics of a lean iso-octane/air mixture under HCCI and SACI conditions, Proc. Combust. Inst. 34 (2013) 2985-2993.

[11] M. B. Luong, Z. Luo, T. Lu, S. H. Chung, C. S. Yoo, Direct numerical simulations of the ignition of lean primary reference fuel/air mixtures with temperature inhomogeneities, Combust. Flame 160 (2013) 2038-2047.

[12] M. B. Luong, T. Lu, S. H. Chung, C. S. Yoo, Direct numerical simulations of the ignition of a lean biodiesel/air mixture with temperature and composition inhomogeneities at high pressure and intermediate temperature, Combust. Flame 161 (2014) 2878-2889.

[13] S. O. Kim, M. B. Luong, J. H. Chen, C. S. Yoo, A DNS study of the ignition of lean PRF/air mixtures with temperature inhomogeneities under high pressure and intermediate temperature, Combust. Flame 162 (2015) 717-726.

[14] M. B. Luong, G. H. Yu, T. Lu, S. H. Chung, C. S. Yoo, Direct numerical simulations of ignition of a lean n-heptane/air mixture with temperature and composition inhomogeneities relevant to HCCI and SCCI combustion, Combust. Flame 162 (2015) 4566-4585.

[15] M. B. Luong, G. H. Yu, S. H. Chung, C. S. Yoo, Ignition of a lean PRF/air mixture under RCCI/SCCI conditions: A comparative DNS study, Proc. Combust. Inst. 36 (2017) 3623-3631.

[16] M. B. Luong, R. Sankaran, G. H. Yu, S. H. Chung, C. S. Yoo, On the effect of injection timing on the ignition of lean PRF/air/EGR mixtures under direct dual fuel stratification conditions, Combust. Flame 183 (2017) 309-321.

[17] N. Peters, Turbulent combustion, Cambridge University Press, 2000.

[18] J. E. Dec, Advanced compression-ignition engine-understanding the in-cylinder processes, Proc. Combust. Inst. 32 (2009) 2727-2742.

[19] L. M. Pickett, Low flame temperature limits for mixing-controlled diesel combustion, Proc. Combust. Inst. 30 (2005) 2727-2735.

[20] C. S. Yoo, R. Sankaran, J. H. Chen, Three-dimensional direct numerical simulation of a turbulent lifted hydrogen jet flame in heated coflow: Flame stabilization and structure, J. Fluid Mech. 640 (2009) 453-481.

[21] C. S. Yoo, E. S. Richardson, R. Sankaran, J. H. Chen, A DNS study on the stabilization mechanism of a turbulent lifted ethylene jet flame in highly-heated coflow, Proc. Combust. Inst. 33 (2011) 1619-1627.

[22] B. C. Choi, K. N. Kim, S. H. Chung, Autoignited laminar lifted flames of propane in coflow jets with tribrachial edge and mild combustion, Combust. Flame 156 (2009) 396-404.

[23] B. C. Choi, S. H. Chung, Autoignited laminar lifted flames of methane, ethylene, ethane, and n-butane jets in coflow air with elevated temperature, Combust. Flame 157 (2010) 2348-2356.

[24] B. C. Choi, S. H. Chung, Autoignited laminar lifted flames of methane/hydrogen mixtures in heated coflow air, Combust. Flame 159 (2012) 1481-1488.

[25] S. K. Choi, S. H. Chung, Autoignited and non-autoignited lifted flames of pre-vaporized n-heptane in coflow jets at elevated temperatures, Combust. Flame 160 (2013) 1717-1724.

[26] S. K. Choi, S. Al-Noman, S. H. Chung, Simulation of non-autoignited and autoignited laminar non-premixed jet flames of syngas in heated coflow air, Combust. Sci. Technol. 187 (2015) 132-147.

[27] S. M. Al-Noman, S. K. Choi, S. H. Chung, Autoignition characteristics of laminar lifted jet flames of pre-vaporized iso-octane in heated coflow air, Fuel 162 (2015) 171-178.

[28] S. M. Al-Noman, S. K. Choi, S. H. Chung, Numerical study of laminar nonpremixed methane flames in coflow jets: Autoignited lifted flames with tribrachial edges and MILD combustion at elevated temperatures, Combust. Flame 171 (2016) 119-132.

[29] S. Deng, P. Zhao, M. E. Mueller, C. K. Law, Autoignition-affected stabilization of laminar non-premixed DME/air coflow flames, Combust. Flame 162 (2015) 3437-3445.

[30] S. Deng, P. Zhao, M. E. Mueller, C. K. Law, Stabilization of laminar nonpremixed DME/air coflow flames at elevated temperatures and pressures, Combust. Flame 162 (2015) 4471-4478.

[31] S. H. Chung, B. J. Lee, On the characteristics of laminar lifted flames in a nonpremixed jet, Combust. Flame 86 (1991) 62-72.

[32] B. J. Lee, S. H. Chung, Stabilization of lifted tribrachial flames in a laminar nonpremixed jet, Combust. Flame 109 (1997) 163-172.

[33] M. de Joannon, A. Saponaro, A. Cavaliere, Zero-dimensional analysis of methane diluted oxidation in rich conditions, Proc. Combust. Inst. 28 (2000) 1639-1646.

[34] A. Cavaliere, M. de Joannon, Mild combustion, Prog. Energy Combust. Sci. 30 (2004) 329-366.

[35] A. Cuoci, A. Frassoldati, T. Faravelli, E. Ranzi, A computational tool for the detailed kinetic modeling of laminar flames: application to C_2H_4/CH_4 coflow flames, Combust. Flame 160 (2013) 870-886.

[36] A. Cuoci, A. Frassoldati, T. Faravelli, E. Ranzi, Numerical modeling of laminar flames with detailed kinetics based on the operator-splitting method, Energy Fuels 27 (2013) 7730-7753.

[37] H. G. Weller, G. Tabor, H. Jasak, C. Fureby, A tensorial approach to computational continuum mechanics using object-oriented techniques, Comput. Phys. 12 (1998) 620-631.

[38] T. F. Lu, C. K. Law, A criterion based on computational singular perturbation for the identification of quasi steady state species: A reduced mechanism for methane oxidation with NO chemistry, Combust. Flame 154 (2008) 761-774.

[39] Y. C. Chen, R. W. Bilger, Stabilization mechanisms of lifted laminar flames in axisymmetric jet flows, Combust. Flame 123 (2000) 23-45.

[40] Y. Xue, Y. Ju, Studies on the liftoff properties of dimethyl ether jet diffusion flames, Combust. Sci. Technol. 178 (2006) 2219-2247.

[41] K. Gkagkas, R. P. Lindstedt, Transported PDF modelling with detailed chemistry of pre- and autoignition in CH_4/air mixtures, Proc. Combust. Inst. 31 (2007) 1559-1566.

[42] R. L. Gordon, A. R. Masri, E. Mastorakos, Heat release rate as represented by [OH]×[CH_2O] and its role in autoignition, Combust. Theory Model. 13 (2009) 645-670.

[43] R. J. Kee, F. M. Rupley, E. Meeks, J. A. Miller, CHEMKIN-III: a fortran chemical kinetics package for the analysis of gas-phase chemical and plasma kinetics, SAND96-8216.

[44] T. Lu, C. S. Yoo, J. H. Chen, C. K. Law, Three-dimensional direct numerical simulation of a turbulent lifted hydrogen jet flame in heated coflow: a chemical explosive mode analysis, J. Fluid Mech. 652 (2010) 45-64.

[45] Z. Luo, C. S. Yoo, E. S. Richardson, J. H. Chen, C. K. Law, T. Lu, Chemical explosive mode analysis for a turbulent lifted ethylene jet flame in highly-heated coflow, Combust. Flame 159 (2012) 265-274.

[46] R. Shan, C. S. Yoo, J. H. Chen, T. Lu, Computational diagnostics for n-heptane flames with chemical explosive mode analysis, Combust. Flame 159 (2012) 3119-3127.

[47] M. B. Luong, G. H. Yu, S. H. Chung, C. S. Yoo, Ignition of a lean PRF/air mixture under RCCI/SCCI conditions: Chemical aspects, Proc. Combust. Inst. 36 (2017) 3587-3596.

[48] A. Lifshitz, K. Scheller, A. Burcat, G. B. Skinner, Shock-tube investigation of ignition in methane-oxygen-argon mixtures, Combust. Flame. 16 (1971) 311-321.

[49] Y. Ju, T. Niioka, Ignition simulation of methane/hydrogen mixtures in a supersonic mixing layer, Combust. Flame. 102 (1995) 462-470.

[50] J. H. Chen, E. R. Hawkes, R. Sankaran, S. D. Mason, H. G. Im, Direct numerical simulation of ignition front propagation in a constant volume with temperature inhomogeneities I. Fundamental analysis and diagnostics, Combust. Flame. 145 (2006) 128-144.

[51] R. L. Gordon, A. R. Masri, S. B. Pope, G. M. Goldin, Transport budgets in turbulent lifted flames of methane autoigniting in a vitiated co-ow, Combust. Flame. 151 (2007) 495-511.

[52] A. Krisman, E. R. Hawkes, M. Talei, A. Bhagatwala, J. H. Chen, Polybrachial structures in dimethyl ether edge-flames at negative temperature coefficient conditions, Proc. Combust. Inst. 35 (2015) 999-1006.

[53] R. W. Grout, A. Gruber, C. S. Yoo, J. H. Chen, Direct numerical simulation of flame stabilization downstream of a transverse fuel jet in cross ow, Proc. Combust. Inst. 33 (2011) 1629-1637.

[54] H. Kolla, R. W. Grout, A. Gruber, J. H. Chen, Mechanisms of flame stabilization and blowout in a reacting turbulent hydrogen jet in cross-ow, Combust. Flame 159 (2012) 2755-2766.

[55] C. K. Law, Combustion Physics, Cambridge University Press, 2006.

Acknowledgements

First and foremost, I would like to express my sincere appreciation to my research advisor, Professor Chun Sang Yoo, for accepting me as a lab member and guiding my research. Without his constant encouragement, this work would not have been possible.

I am also grateful to all member of our laboratory. All of them give me invaluable ideas which can broaden my view, and they make the best surroundings for me to adopt the life in UNIST. Every moment that I spent with them will not be forgettable.

I always thanks to my family who respect my decision to enter the graduate school. Without their untiring love and support, I would not be here.